YBCO hot-electron bolometers dedicated to THz detection and imaging: Embedding issues

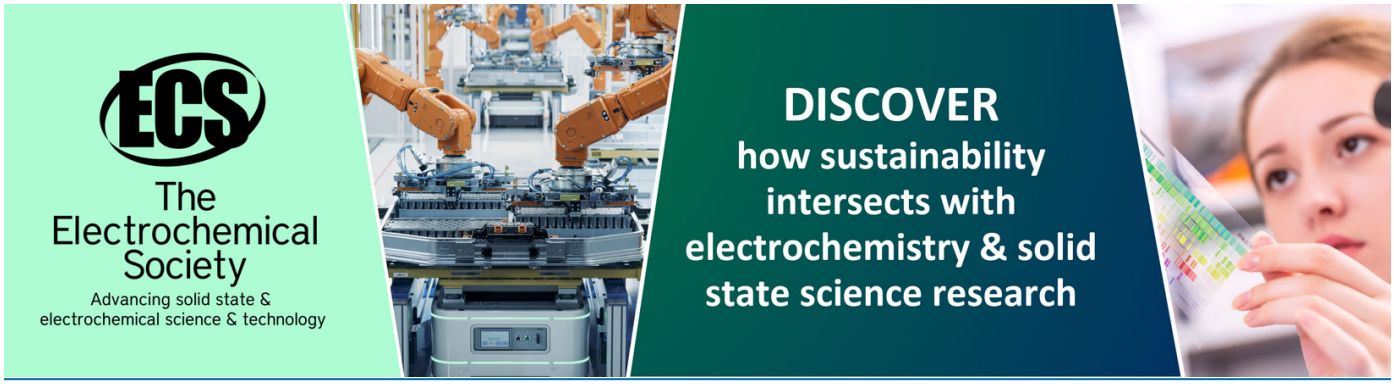

Journal of Physics: Conference Series **234** (2010) 042002 doi:10.1088/1742-6596/234/4/042002

YBCO hot-electron bolometers dedicated to THz detection and imaging: embedding issues

M Aurino, A J Kreisler[1], I Türer, A Martinez, A Gensbittel and A F Dégardin

LGEP; SUPELEC; UMR CNRS 8507; UPMC Univ Paris 06; Univ Paris Sud 11;
11 rue Joliot-Curie, Plateau de Moulon, 91190 Gif-sur-Yvette, France.

E-mail: Alain.Kreisler@supelec.fr

Abstract. High-T_c hot-electron bolometers (HEB) are an interesting alternative to other superconducting heterodyne mixers in the terahertz frequency range because of low-cost cooling investment, ultra-wide instantaneous bandwidth and low intrinsic noise level, even at 80 K. A technological process to fabricate stacked yttrium-based (YBCO) / praseodymium-based (PBCO) ultra-thin films (in the 15 to 40 nm thickness range) etched to form 0.5 μm × 0.5 μm constrictions, elaborated on (100) MgO substrates, has been previously described. Ageing effects were also considered, with the consequence of increased electrical resistance, significant degradation of the regular THz response and no HEB mixing action. Electron and UV lithography steps are revisited here to realize HEB mixers based on nano-bridges covered by a log-periodic planar gold antenna, dedicated to the 1 to 7 THz range. Several measures have been attempted to reduce the conversion losses, mainly by considering the embedding issues related to the YBCO nano-bridge impedance matching to the antenna and the design of optimized intermediate frequency circuitry. Antenna simulations were performed and validated through experiments on scaled models at GHz frequencies. Electromagnetic coupling to the incoming radiation was also studied, including crosstalk between neighbour antennas forming a linear imaging array.

1. Introduction

There is a strong need for wideband and sensitive receivers for radio astronomy and remote sensing applications in the terahertz (THz) region. The emergence of nanotechnologies has raised a large interest in superconducting detectors for terahertz applications, as a substitute to Schottky diode mixers. Hot-electron bolometer (HEB) detectors using very thin superconducting film structures in the transition state have also emerged as a competitive alternative to the traditional Superconductor-Insulator-Superconductor (SIS) mixers used in the THz range.

Data concerning the most popular THz heterodyne receivers are shown in figure 1. In particular, one can observe the frequency limitation of SIS devices due to the superconducting gap, the Schottky sensitivity limitation and the good sensitivity of low-T_c superconducting (LTS) film HEBs over a large wavelength range. The recently launched (May 2009) Herschel space probe is currently running LTS HEB receivers covering the 157–213 μm wavelength range in its HIFI instrument [1].

[1] To whom any correspondence should be addressed.

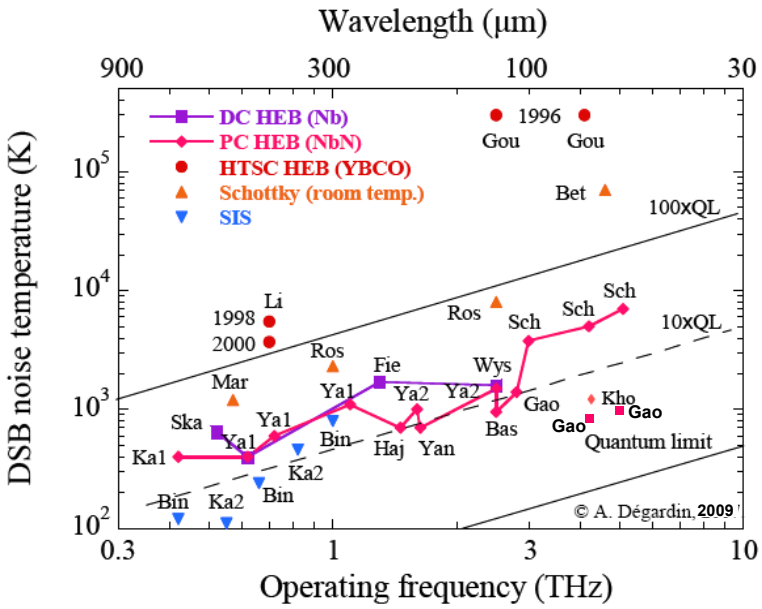

Figure 1. Double sideband (DSB) noise temperature as a function of operating frequency (or wavelength in the vacuum) for various heterodyne receivers (after [2], updated). For YBCO HEBs, "Gou" and "Li" labels apply to [3] and [4], respectively. For low-T_c HEBs, "DC" and "PC" mean "diffusion cooled" and "phonon cooled", respectively. Quantum limit (QL) states for hf/k_B.

The first published data on high-T_c superconducting (HTS) THz HEBs with $YBa_2Cu_3O_{7-\delta}$ (YBCO) films are also shown in figure 1. Although falling short of performance expectations, mainly related to YBCO nanostructuration challenges, it should be stressed that Karasik *et al.* [5] predicted ~ 2000 K (single sideband) noise temperature at 2.5 THz for an YBCO mixer operating at 66 K (readily obtainable with a lightweight cryocooler) with 11 μW local oscillator (LO) power (to be compared with the several mW required by Schottky mixers).

A HEB THz detector typically consists of an ultra-thin (i.e. a few 10 nm thick) superconducting constriction of sub-μm dimensions coupled to the THz radiation by means of a planar antenna. The ultimate bandwidth of a HTS HEB is determined by the electron-phonon scattering rate, which is about 1.5 to 5 ps at 80 - 90 K in YBCO, and so makes it an ideal candidate to achieve several tens of gigahertz intermediate frequency (IF) in heterodyne receivers.

In the following, we shall briefly recall in section 2 our initial fabrication process of YBCO constrictions, their integration in THz detectors/mixers, and mention the difficulties encountered in terms of ageing and losses at both input (THz antenna) and output (IF GHz circuitry) ports. We shall then indicate in section 3 a new technological approach to optimize the device overall performance with respect to those issues. Section 4 will deal with THz antennas and IF circuitry (HEB embedding circuitry) and linear imaging array concepts.

2. The initial HEB fabrication process

Our initial process to fabricate HEB devices followed from ultra-thin YBCO/PBCO ($PrBa_2Cu_3O_{7-\delta}$) multilayer elaboration expertise [6] and device simulations for optimal constriction dimensions [7]. The main steps can be summarized as follows [8-10].

- Sequential inverted (hollow) cathode sputter deposition of [PBCO (2 to 4 nm) - YBCO (12 to 40 nm) - PBCO (2 to 4 nm)] trilayers on 250 μm thick (100) MgO substrates.

- *ex situ* DC sputtering of 300 nm thick gold contact pads through a mechanical copper mask.
- Initial patterning of the PBCO/YBCO/PBCO tri-layers using e-beam lithography to form narrow lines, in order to define the length of the constriction.
- Xenon ion beam milling of this feature.
- Regular optical lithography to complete the definition of the micro-bridge structure.
- Defining the constriction width by xenon ion milling using patterned photoresist as a mask.
- Patterning of a DC sputtered gold metal wideband planar antenna (300 nm thickness) of the log-periodic type by using a lift-off technique.

Typical optical micrographs of a device and its environment are shown in figure 2. As mentioned in previous papers, these concepts proved the validity of the whole process insofar as the superconducting properties of the constriction were concerned, but also arose ageing effects that prevented to demonstrate THz HEB action, only allowing to observe direct detection at 2.5 THz with low sensitivity due to losses arising both at front end as well as back end device terminals [11,12]. These losses were attributed to excess trilayer areas introducing spurious ohmic losses at the antenna centre in the one hand and output path in the other.

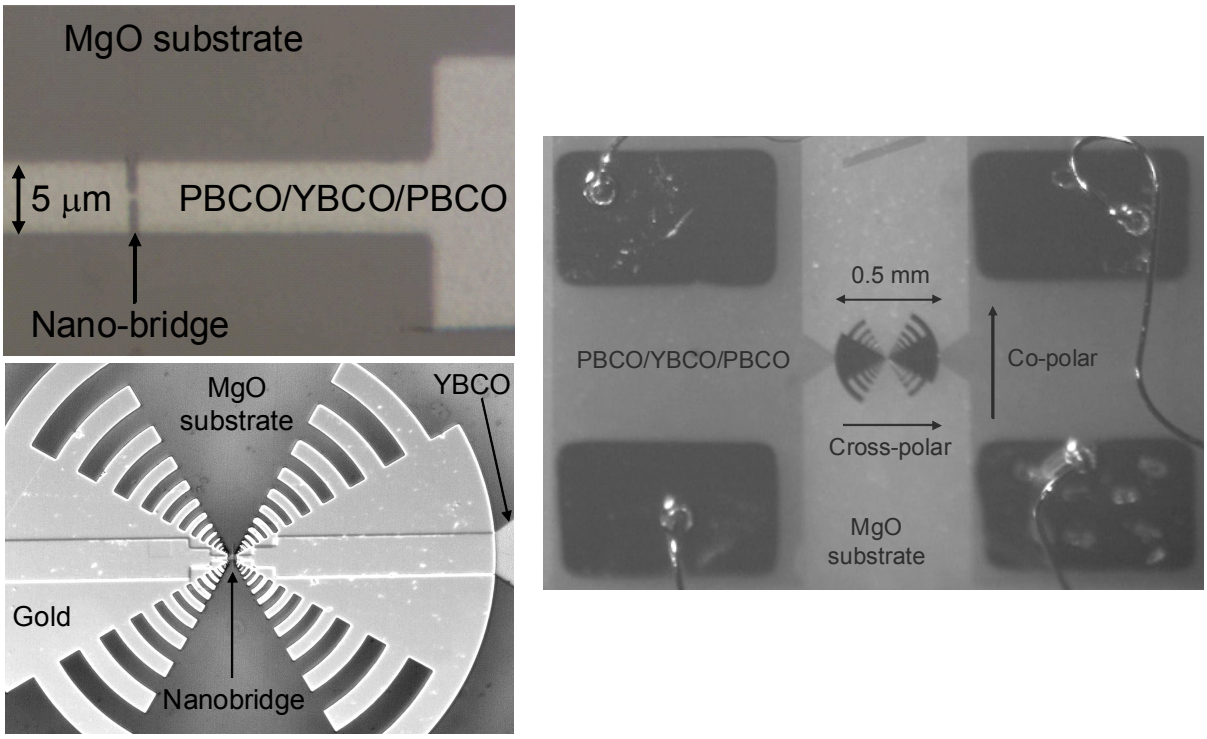

Figure 2. Top left: A 40×5 μm^2 micro-bridge patterned on a PBCO (4 nm) - YBCO (15 nm) - PBCO (4 nm) trilayer. The e-beam defined constriction (nano-bridge) is 0.8×0.8 μm^2 [11].

Bottom left: Optical micrograph showing gold log-periodic antenna (outer diameter: 500 μm, inner diameter: 9.5 μm) on top of PBCO/YBCO/PBCO trilayer [11]. The narrow line defining the nano-bridge can be guessed at the antenna centre.

Right: The tested device, with DC bias and output signal gold pads and wiring, gold antenna and trilayer structure [12]. The THz field conventional directions for co- and cross-polarization are indicated.

3. The new HEB fabrication process

3.1. The antenna centre

As shown in the previous design (figure 2), four contact pads were realized for electrical characterization, device electrical biasing and output signal monitoring. With this configuration the distance between the contacts and the centre of the bridge is about 1 mm as shown in figure 3. The YBCO trilayer electrical path length leading to the centre of the device is therefore much longer than that of the metal contacts. For this reason a main contribution to the total resistance arises from the YBCO bridge part. We can calculate the contribution arising from this part by considering its length of 40 µm, its width of 5 µm and the sample thickness of (e.g.) 40 nm. On this micro-bridge section, a constriction of 0.7×0.7 µm^2, typically, is created by electronic lithography at its centre. So the total resistance of the bridge can be considered as the sum of the contribution coming from zone 1 (constriction) and zone 2 (remaining part of the micro-bridge).

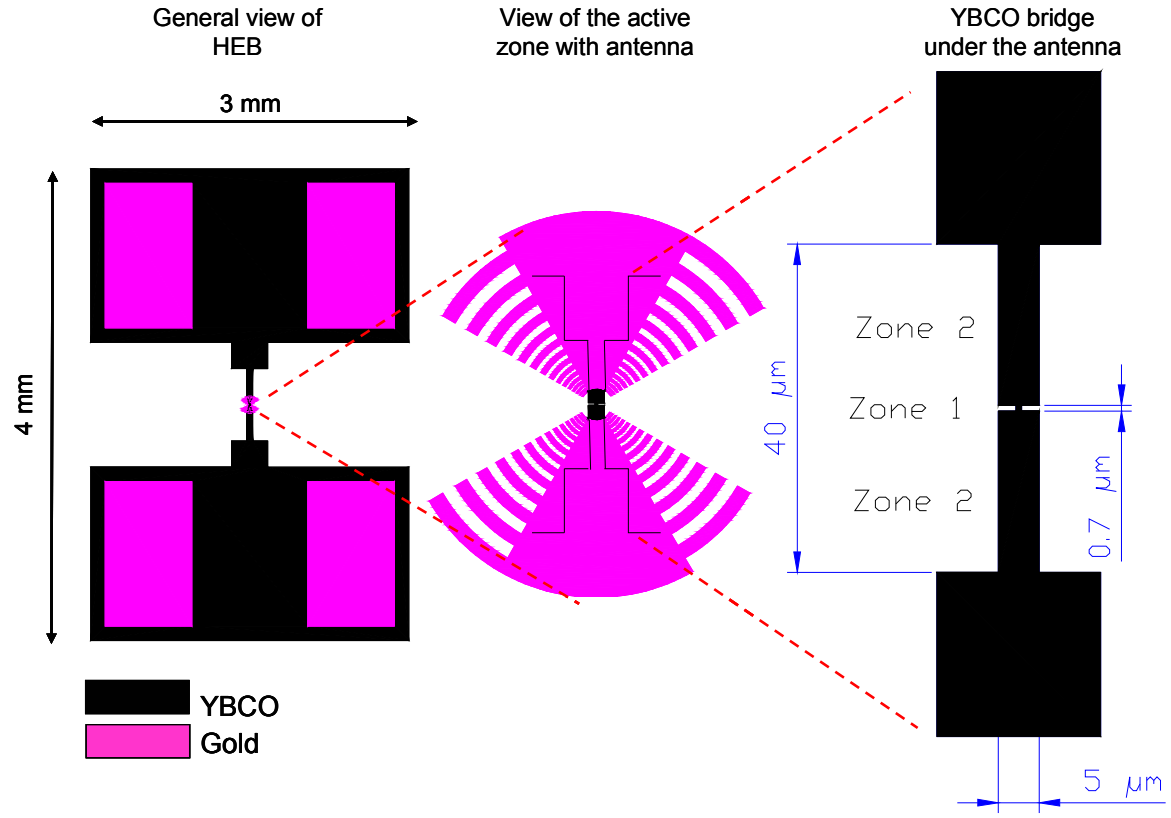

Figure 3. First configuration (see figure 2). The distance between the contact pads and the centre of the antenna is about 1 mm. The main contribution to the total resistance of the bridge comes from the centre of the bridge included between the two halves of the antenna.

In our new design, two contact pads have been added at the antenna centre so the distance between them represents the length of the bridge (see figure 4). These contacts can be realized either by using optical lithography or e-beam lithography. With optical lithography, we can expect a resolution down to 2 µm, whereas with e-beam it is possible to realize a separation between the contacts down to 300 nm. In this latter case, the resistance of the bridge arises only from the constriction contribution (zone 1) whereas for the contacts obtained with optical lithography, a small contribution coming from the YBCO material remaining between the constriction and the contacts should be added (zone 2).

3.2. Evaluating the loss reduction

In order to have an idea of the resistance reduction arising from these configurations we can evaluate the total resistance R_{tot} of the micro-bridge and constriction by considering a bridge without antenna. We neglect the contribution arising from the wide parts of the bridge for the first design (figure 3): In this case we only consider the contributions arising from the narrowest part obtained from optical lithography (zone 2) and the constriction (zone 1). The length of the bridge for the first process is 40 µm and the width is 5 µm. We also assume the same size of the constriction (0.7×0.7) µm^2 made on a 40 nm thick YBCO trilayer for both designs.

The evaluation was performed for the configuration of the first design (figure 3) and the three cases of the second design (figure 4) using the basic relationship:

$$R_{tot} = R_1 + 2R_2 = \rho\left(\frac{l_1}{S_1} + 2\frac{l_2}{S_2}\right) \quad (1)$$

where ρ is the trilayer electrical resistivity, R_i, l_i, S_i are the resistance, length and cross section, respectively, for zone 1 (i = 1) and zone 2 (i = 2).

For the new design, we have considered three cases (see figure 4):

- *Case a*): The distance between the contacts obtained with optical lithography is 2 µm.
- *Case b*): The distance between the contacts is 0.7 µm (obtained with e-beam lithography), in this case the resistance arising from zone 2, $R_2^{design2} = 0$.
- *Case c*): The distance between the contacts is 0.3 µm (close to the resist resolution limit).

The results of the evaluation are gathered in table 1. The reduction of the normal state resistance of the bridge with the second design is between 7 and 21 times with respect to the first design value. The advantage arising from the reduction of the distance between the contacts is evident; it means that the mismatch conversion loss can thus be reduced by an amount ranging from 3.6 to 7.5 dB.

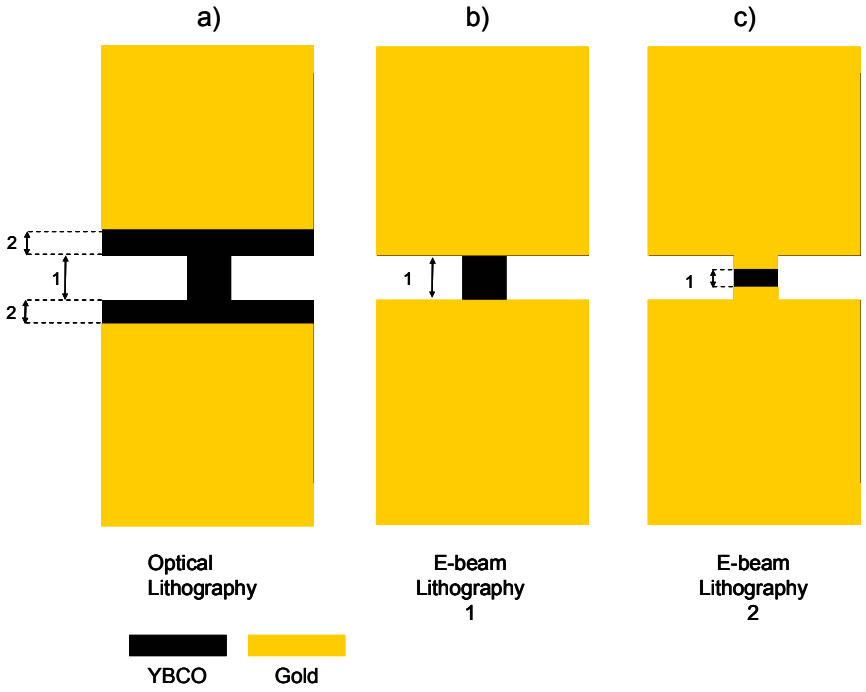

Figure 4. The different solutions for the contact realization with the second design. Numbers 1 and 2 mark YBCO zones of different lengths between the contact pads.

Table 1. Evaluation of the bridge resistance for first and second design (see figure 4). The improvement factor with respect to our initial design is given in the last column.

Configuration	l_1 (μm)	l_2 (μm)	S_1 (nm^2)	S_2 (nm^2)	R_{tot}	$R_{tot}^{design\ 1} / R_{tot}^{design\ 2}$
First design	0.7	39.3	40×700	40×5000	ρ×22.15	1
Second design (a)	0.7	1.3	40×700	40×5000	ρ×3.15	7.03
Second design (b)	0.7	0	40×700	0	ρ×2.5	8.9
Second design (c)	0.3	0	40×700	0	ρ×1.05	20.7

4. HEB embedding circuitry and linear array concept

4.1. Antenna concept in the new design

In the new design, we kept a log-periodic antenna scheme, because of its high directivity and independence of the impedance on the operating frequency. We used the gained experience in the fabrication of the antenna with the first process to define more realistic sizes from the technological point of view. In fact, in the previous process we had some problems with the lift-off of the smallest teeth of the antenna because of their sub-micrometre size, so below our optical lithography limits. Moreover these teeth correspond to very high frequencies (9-10 THz). As the laser sources available for our THz characterization are fixed at about 2.5 THz, our interest has been focused on an antenna with a reduced bandwidth with respect to the first one but having a high level of definition for the teeth corresponding to the frequency of the laser source.

The new antenna design is detailed in [13]. The antenna electromagnetic behaviour was simulated in the THz frequency range with a finite element software (CST Microwave Studio®). A large-scale model in the microwave range (× 400 by wavelength) was fabricated and tested in an anaechoic chamber for cross-validation purpose. The external radius of the antenna has been reduced down to 58.1 μm (instead of 250 μm in the previous design), the inner radius increased up to 7.5 μm (instead of ≈ 4.8 μm) and the smallest tooth (and the smallest tooth separation) size has been increased up to 1.1 μm (instead of ≈ 0.7 μm), for a bandwidth range spanning from 0.9 to 7 THz.

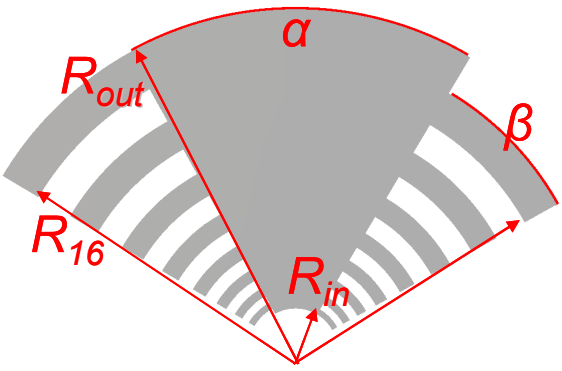

Figure 5. Log-periodic antenna (1 half) in 8-teeth self-complementary configuration ($\alpha + \beta = 90°$).

Table 2. Log-periodic antenna parameter values for 0.9 to 7 THz bandwidth.

Parameter		Values
Inner radius	R_{in}	7.5 μm
Outer radius	R_{out}	58.1 μm
Radii ratio parameter	τ	1.1365
Flare angle	α	60°
Arm angle	β	30°

The antenna geometry is shown in figure 5 and the numerical parameters are given in table 2. In this way the teeth resonating at 2.5 THz are large enough to be realized with a good resolution and far from the external radius where the antenna geometry (and then the radiation pattern) can be altered by the presence of the propagation line that collects the microwave signal (see next sub-section).

4.2. Collecting the IF microwave signal

In order to collect the signal at the microwave intermediate frequency from the centre of the bridge the antenna has been integrated into a microstrip line which carries the signal towards the edge of the substrate. This scheme allows avoiding extra conversion loss arising from "useless" YBCO material in series with the IF load in the initial process (see figure 2, right). For a 50 Ω load and aged YBCO, the IF losses can be consequently reduced by 5.5 dB.

The microstrip line, which is connected to the external radius of the antenna, has its characteristic impedance given by [14]:

$$Z_0 = \frac{120\pi}{\varepsilon_{eff} \times \left[\frac{W}{H} + 1.393 + \frac{2}{3}\ln\left(\frac{W}{H} + 1.444\right)\right]} \quad (2)$$

where ε_{eff} is the effective permittivity, W is the width of the microstrip and H the thickness of the substrate. For a 300 μm wide microstrip line deposited on a 250 μm thick MgO substrate (ε_r = 10) we obtain an impedance value Z_0= 44.4 Ω.

The microstrip is enlarged up to 500 μm at the edge of the substrate (which gives an impedance value of 33 Ω) for making the bonding easier. In the design of the line, we tried to find a trade-off between the feasibility of the line and the corresponding impedance. It was not possible to add an impedance matching configuration because we do not know the exact impedance of the bridge to be adapted. However, we can vary the impedance of the bridge by changing the working temperature of the device in order to have a better matching.

4.3. Linear pixel array design

The simplest linear array demonstrator is constituted of 3 pixels, as shown in figure 6.

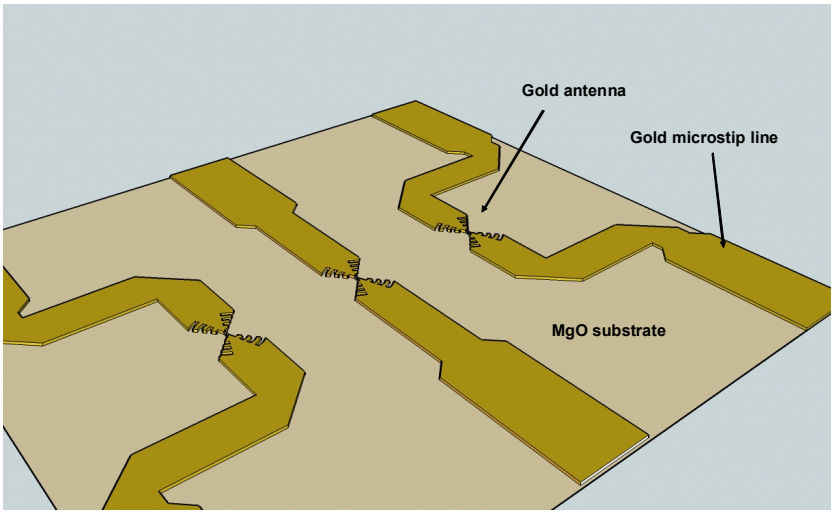

Figure 6. Scheme of an array of three HEBs. Each antenna is integrated into an output IF microstrip line. The microstrip lines on the sides are bent in order to reach the position of the coplanar lines carrying the IF signals to the output SMA connectors.

The reduction of the distance between the pixels for an imaging device is synonymous of better resolution but the final separation is normally a trade-off arising from several considerations. From the optical point of view, the overlap of the Airy discs relative to the beam focusing on two neighbour pixels is to be avoided. According to the Rayleigh criterion, we have:

$$x = 1.22 \frac{\lambda f_L}{d} \tag{3}$$

where x is the separation of the images of the two objects, λ is the radiation wavelength, d is the lens diameter and f_L is the distance from the lens to the sensing film, considered approximately equal to the focal length of the lens. Pixels of the image sensor closer than x would not actually increase image resolution. In our case we use a semi-spherical lens (of diameter 13 mm and focal length 3 mm) which, according to the above equation gives x = 34 μm for a 2.5 THz signal; this value is actually much smaller than the antenna diameter (~ 116 μm).

Moreover the effect of the electromagnetic crosstalk between pixels should be taken into account. Simulations using Sonnet® were performed to check the crosstalk between adjacent lines. The tested configuration is shown in figure 7a, with the IF input/output port numbers. The lines (of width 300 μm) have been placed at two different distances d_{13} = 500 μm and d_{15} = 350 μm.

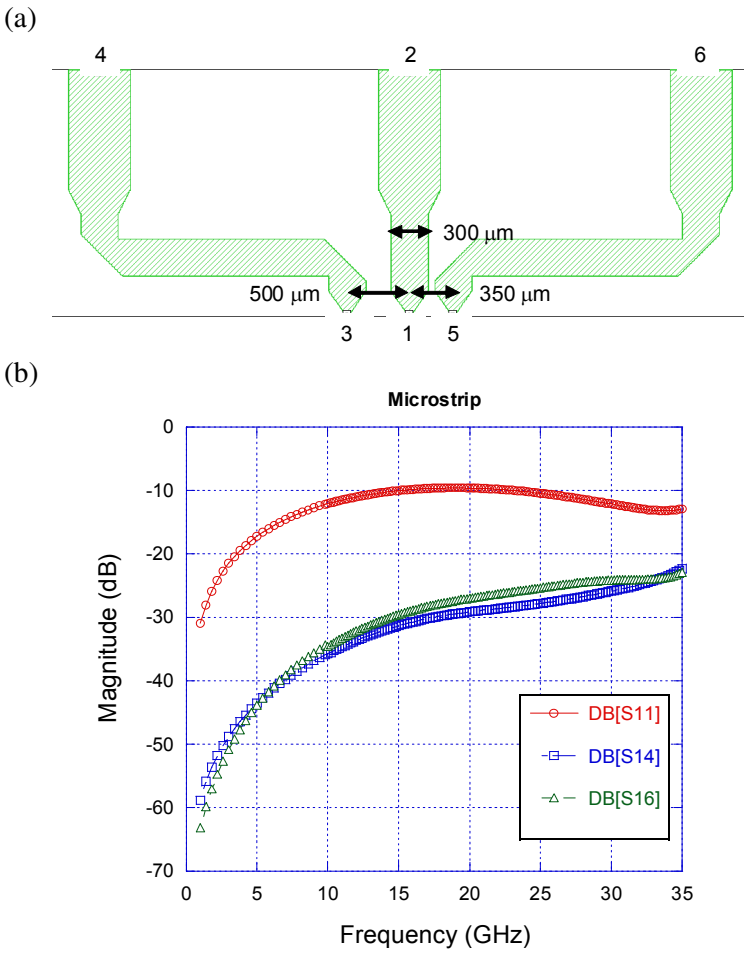

Figure 7. (a): Configuration to check the reflection coefficient and crosstalk between adjacent lines, with port numbers indicated (see text). (b): Results for reflection coefficient (upper curve) and crosstalk (lower curves).

In figure 7b the circles represent the results of the simulation for the reflection of the central line. In the range up to 35 GHz the signal is almost completely transmitted (more than 90 %), the reflection contribution can be neglected. The crosstalk between the lines was also analyzed. We fed the line in port 1 and measured the signal in ports 4 and 6 at the extremity of the other two lines. We found encouraging values, mainly below –25 dB, a negligible crosstalk between the lines even for a 350 μm spacing.

Another point to be investigated in the three-pixel configuration was the study of the electromagnetic crosstalk between antennas, which has been simulated by using CST Microwave Studio®. One antenna was fed in the 0 to 5 THz range and the electromagnetic propagation was measured at the level of the second antenna at a distance of 400 μm (distance between the antennas in the standard three-pixel configuration). The result of this simulation is shown in figure 8 where the behaviour of the measured signal on the second antenna is plotted as a function of the frequency. A value below –20 dB was obtained through the whole antenna bandwidth (0.9 to 7 THz), indicating a negligible electromagnetic crosstalk.

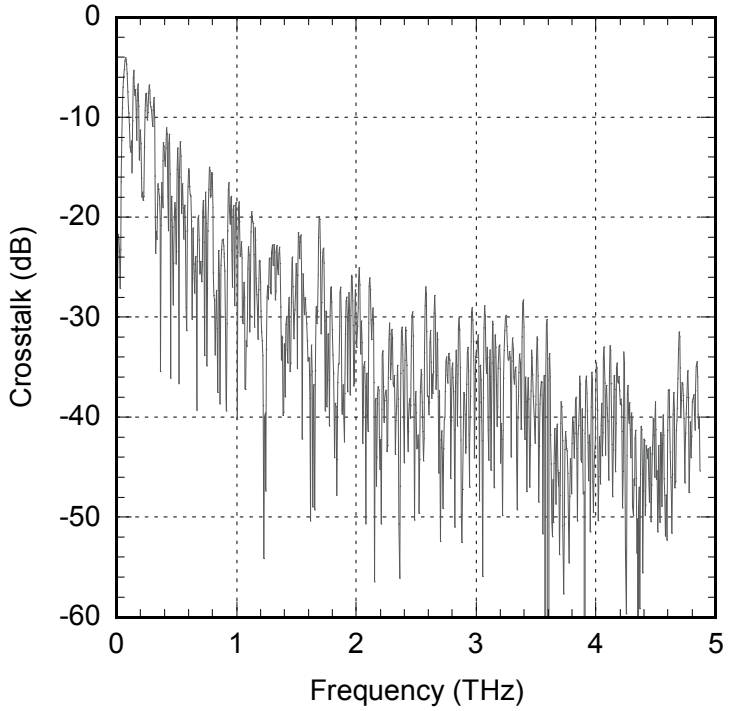

Figure 8. Behaviour of the electromagnetic crosstalk simulated for two log-periodic antennas separated by 400 μm (~ 3.5 × antenna outer diameter).

Conclusion

Following early studies on YBCO devices designed for HEB action at THz frequencies, design technology and engineering concepts have been revisited to lessen the impact of formerly observed ageing effects and excess losses. The new design allows to minimize the YBCO material area in contact with the outer atmosphere, so avoiding detrimental effects arising from water vapour and carbon dioxide, namely a progressive increase of the electrical resistance. At the same time, limiting the YBCO useless (and eventually aged) material on both the RF (antenna centre) and IF output paths allows to potentially reduce by up to 13 dB the mixer conversion loss (7.5 dB RF and 5.5 dB IF). Finally, a simple three-pixel linear array scheme is proposed as a first demonstrator of high-T_c THz imager.

Acknowledgments
The authors are grateful to Dr JC Villegier for advice and availability of clean room equipment at CEA-INAC Grenoble. This research project has been supported by a Marie Curie Early Stage Training Fellowship of the European Community's Sixth Framework Programme under contract number MEST-CT-2005-020692. It has been partly supported by the French government agency for space studies (CNES) under Contract 60587/00 and by specific funding from UPMC Univ Paris 06.

References
[1] http://herschel.esac.esa.int/
[2] Kreisler A and Gaugue A 2000 *Supercond. Sci. Technol.* **13** 1235
[3] Gousev Y P, Semenov A D, Pechen E V, Varlashkin A V, Nebosis R S and Renk K F 1996 *Supercond. Sci. Technol.* **9** 779
[4] Li C-T, Deaver B S Jr, Lee M, Weikle R M II, Rao RA and Eom CB 1998 *Appl. Phys. Lett.* **73** 1727
[5] Karasik B S, McGrath W R and Gaidis M C 1997 *J. Appl. Phys.* **81** 1581
[6] Jaeger A, Villégier J-C, Bernstein P, Bok J and Force L 1993 *IEEE Trans. Appl. Supercond.* **3** 2993
[7] Adam A, Gaugue A, Ulysse C and Kreisler A J 2002 *IEEE Trans. Appl. Supercond.* **13** 155
[8] Villégier J-C, Dégardin A F, Guillet B, Houzé F, Kreisler A J and Chaubet M 2005 *Terahertz and Gigahertz Electronics and Photonics IV*: SPIE Vol. 5727 Ed R J Hwu and K J Linden pp. 88–94
[9] Péroz Ch, Villégier J-C, Dégardin A F, Guillet B and Kreisler A J 2006 *Appl. Phys. Lett.* **89** 14502
[10] Aurino M, Villégier J-C, Dégardin A F, Guillet B and Kreisler A J 2007 *J. of Physics, conference series*: http://www.iop.org/EJ/toc/1742-6596/97/1, paper 012075
[11] Péroz Ch, Dégardin A F, Villégier J-C and Kreisler A J 2007 *IEEE Trans. Appl. Supercond.* **17** 637
[12] Kreisler A J, Dégardin A F, Aurino M, Péroz Ch., Villégier J-C, Beaudin G, Delorme Y, Redon M and Sentz A 2007 *Proc. IEEE International Microwave Symposium (Honolulu, Hawaii, USA, 3-8 June 2007)* pp. 345-348
[13] Türer I, Gaztelu X, Ribière-Tharaud N, Degardin A F and Kreisler A J 2010 *Ultra-wideband, Short-Pulse Electromagnetics 9* Ch. 21 Ed F Sabath *et al* (Springer) pp. 201-210
[14] Bahl I J and Trivedi D K 1977 *Microwaves* **16** 174